Science of the Total Environment 554–555 (2016) 228–236

Contents lists available at ScienceDirect

Science of the Total Environment

journal homepage: www.elsevier.com/locate/scitotenv

Application of a multi-method approach in characterization of natural aquatic colloids from different sources along Huangpu River in Shanghai, China

Caixia Yan [a,b,c], Minghua Nie [a], Jamie R. Lead [b], Yi Yang [c,d], Junliang Zhou [c], Ruth Merrifield [b], Mohammed Baalousha [b,*]

[a] School of Geography and Environment, Key Laboratory of Poyang Lake Wetland and Watershed Research, Ministry of Education, Jiangxi Normal University, 99 Ziyang Road, Nanchang 330022, China
[b] Center for Environmental Nanoscience and Risk, Arnold School of Public Health, University of South Carolina, 921 Assembly Street, Columbia 29208, USA
[c] State Key Laboratory of Estuarine and Coastal Research, East China Normal University, 3663 North Zhongshan Road, Shanghai 200062, China
[d] Key Laboratory of Geographic Information Science of the Ministry of Education, Department of Geosciences, East China Normal University, 3663 North Zhongshan Road, Shanghai, 200062, China

HIGHLIGHTS

- Natural aquatic colloids from different sources were isolated using cross flow ultrafiltration.
- Multi-method approach is applied for colloidal characterization.
- Colloids in pristine natural river water showed higher aromaticity, humification, fluorescent intensity, and smaller sizes.
- Optical properties of colloids are size-dependent.

GRAPHICAL ABSTRACT

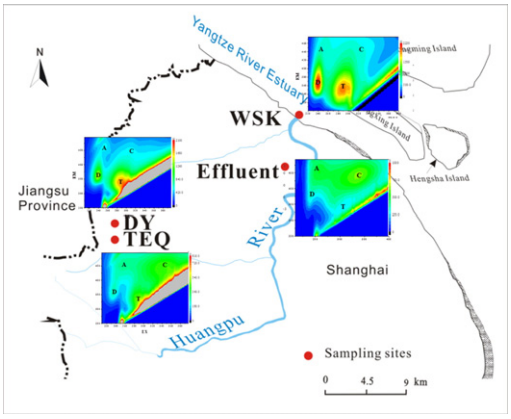

ARTICLE INFO

Article history:
Received 11 January 2016
Received in revised form 27 February 2016
Accepted 28 February 2016
Available online 5 March 2016

Editor: D. Barcelo

Keywords:
Colloids
Absorbance
Fluorescence

ABSTRACT

Natural colloid properties and the impact of human activities on these properties are important considerations for studies seeking to understand the fate and transport of pollutants. In this study, the relationship between size and fluorescence properties of natural colloids from 4 different sources were quantified using a multi-method analytical approach including UV–visible and fluorescence spectroscopy, flow field flow fractionation (FlFFF) coupled online to fluorescence spectrometer, and atomic force microscopy (AFM). Results indicate that colloids from pristine natural river water have higher aromaticity and humification, higher fluorescent intensity, and smaller size compared to those from the rivers impacted by livestock. The majority of colloids are smaller than 10 nm in size as measured by AFM and FlFFF. Colloid size measured by FlFFF coupled to fluorescence spectroscopy increases in the order peak C (Ex/Em at 300–340/400–460 nm) < peak D (Ex/Em at 210–230/340–360 nm) < peak T (Ex/Em at 270–280/330–370 nm) < peak A (Ex/Em at 210–250/400–460 nm), revealing that optical properties such as fluorescence are correlated with size. This trend is confirmed by the principal compo-

* Corresponding author.
E-mail address: MBAALOUS@mailbox.sc.edu (M. Baalousha).

http://dx.doi.org/10.1016/j.scitotenv.2016.02.198

Size distribution
Principle component analysis (PCA)

nent analysis, which demonstrates that the first principal component (PC1) reflecting colloid optical properties decrease with the increase in PC3 which is correlated to the colloid size.

1. Introduction

Aquatic colloids are heterogeneous mixtures of particles with different sizes, shapes, coatings, surface chemistry and chemical composition, and are defined as solid materials with at least one dimension between 1 nm and 1 μm (Lead and Wilkinson, 2006; Wilkinson and Lead, 2007). Colloids in natural systems are generally derived from natural processes, such as volcanic eruptions and bacterial activity, or anthropogenic activities such as wastewater treatment plants (WWTPs) effluent, livestock wastewater, or their distribution systems (Buzea et al., 2007). Colloid properties play important roles in regulating the fate and behavior of contaminants in the aquatic environment (Kalmykova et al., 2013; Nie et al., 2014a; b). It has been established that small size, high organic carbon content and high humic-like fluorescence intensity of natural aquatic colloids are among the main factors controlling pollutant–colloid interactions such as sorption behavior (e.g. pesticide, estrogens and pharmaceuticals) (Ngueleu et al., 2013; Nie et al., 2014a; b; Yan et al., 2015).

There are strong indications that the geochemical composition and properties of colloids vary with size (Khalaf et al., 2003). Understanding the relationship between colloidal composition and size distribution requires improvement in colloid separation and analysis using a hyphenated multi-method approach. Several analytical techniques such as cross-flow ultrafiltration (CFUF), flow field flow fractionation (FlFFF) (Laborda et al., 2011; Batchelli et al., 2009), atomic force microscopy (AFM)(Baalousha and Lead, 2007a; Wilkinson et al., 1999), and inductively coupled plasma mass spectrometry (ICP-MS) (Stolpe et al., 2005) have been applied for the characterization of colloids. However, due to the profound complexity, heterogeneity and polydispersity of colloids, there is a need for in-depth characterization of colloids using a multi-method approach to quantify their properties (Lapworth et al., 2013; Yang et al., 2015), in particular applying high resolution size separation techniques such as FlFFF, prior to further characterization using other analytical techniques to reduce colloid polydispersity and thus improve detection of subtle differences in colloid properties (Weishaar et al., 2003). As an important portion of colloid, properties of the chromophoric dissolved organic matter (CDOM) have been shown to be size-dependent (Guéguen and Cuss, 2011). For instance, in samples from an urban lake and a rural river, tryptophan-like fluorescence and a small fraction of fulvic-like fluorophores occurred mainly in the dissolved phase (permeates), while humic/fulvic-like materials primarily occurred in the concentrated colloidal phase (retentates) (Liu et al., 2007). However, there is little information on the relationship between fluorescence and size of colloids and the results are contradictory. For example, the humic-like fluorescent fraction of DOM is usually found in the range 0.5–5 kDa in pristine natural waters (Thurman, 1985; Huguet et al., 2010), but in the Damariscotta River estuary, Boehme and Wells (2006) detected fluorescence in larger sized fraction 13–150 kDa. These differences can be attributed to the different techniques and methodologies applied in the different studies, sample origin, and colloid polydispersity.

Therefore, to overcome these challenges, a range of complementary methods were selected in this study to characterize the colloids, including UV–visible and fluorescence spectroscopy, FlFFF coupled online to fluorescence spectroscopy, and AFM. Absorption and fluorescence spectroscopy are powerful tools to identify the colloidal component and assess the sources and dynamics of natural colloids (Persson and Wedborg, 2001; Hong et al., 2012). FlFFF measures colloids diffusion coefficient, which can be converted to colloid hydrodynamic diameter using Stocks Einstein equation, with the inherent assumption that these colloids are hard-spheres, although comparison of data from the two methods can yield information on colloidal softness (permeability)(Baalousha and Lead, 2007a). FlFFF has been coupled with several detectors such as fluorescence, light scattering, AFM, and ICP-MS (Wyatt et al., 1998; Baalousha and Lead, 2007a; Bouby et al., 2008) to characterize the continuous molecular size information of colloids and their interaction with pollutants (Guéguen and Cuss, 2011; Cuss and Guéguen, 2015). AFM measures colloidal height above a substrate, which are typically used to construct colloid size distribution assuming spherical shape. Crucially, FlFFF and AFM operate at the same nanoscale size, but are based on different basic principles as discussed above, and are thus highly complementary for colloid characterization. Coupling of both methods enables the validation of the Stokes Einstein assumption (Baalousha and Lead, 2007a,b; Lapworth et al., 2013).

For FlFFF analysis, both UV and fluorescence detector have been coupled to FlFFF in previous studies (Moon et al., 2006; Baalousha and Lead, 2007a; Guéguen and Cuss, 2011; Lapworth et al., 2013). However, measured size distributions were different between absorbance and fluorescence, because chromophores did not have the same size distribution as the fluorophores, especially for the larger sized colloids in rivers and coastal waters (Zanardi-Lamardo et al., 2004; Guéguen and Cuss, 2011). Furthermore, the results from fluorescence are sampled dependent. No significant variation in colloid size distribution was observed in the analysis of protein-like materials (Moon et al., 2006), while significant variation in colloidal size distribution were identified when using the fluorescence signal for humic material (Hassellöv, 2005). These findings illustrate that fluorescence signatures might be size-dependent. Thus to rationalize the variability in the colloid size-dependent optical properties (fluorescence), it is necessary to couple FlFFF to a fluorescence detector with various wavelengths. Therefore, according to the fluorophores measured in the batch fluorescence analysis (see details in the following discussions), four Ex-Em pairs representing fulvic-like, protein-like, tryptophan-like and humic-like materials were selected in this study to monitor colloidal size distribution following fractionation by FlFFF. This is one of the very few studies that demonstrate the difference in colloidal size distribution by FlFFF at different fluorescence wavelengths.

In this study, colloids were collected from different sources including the confluence of rivers, effluent of WWTP, and rivers impacted by livestock in Shanghai, China (Fig. 1). The objectives of this paper are to optimally couple multiple techniques, and to systematically assess the relationships of properties (e.g. fluorescence vs. size) of aquatic colloids, and the impact of human activities on colloid properties. To achieve this goal, we (1) determine the absorbance, fluorescence and size distribution of colloids from different sources; (2) investigate the relationship between fluorescence and size distribution using FlFFF analysis; and (3) extract the latent variables from several parameters of colloids using principal component analysis (PCA). Latent variables were in turn used to predict size distribution using only the fluorescence properties thereof.

2. Materials and methods

2.1. Sample collection

Four water samples were collected from different sources along the Huangpu River in Shanghai, China (Fig. 1). Of these sampling sites, Wusongkou (WSK) is the confluence of the Huangpu River and the Yangtze River, representing the overall effect of the human activity and the pristine natural process; “Effluent” is the final effluent of an

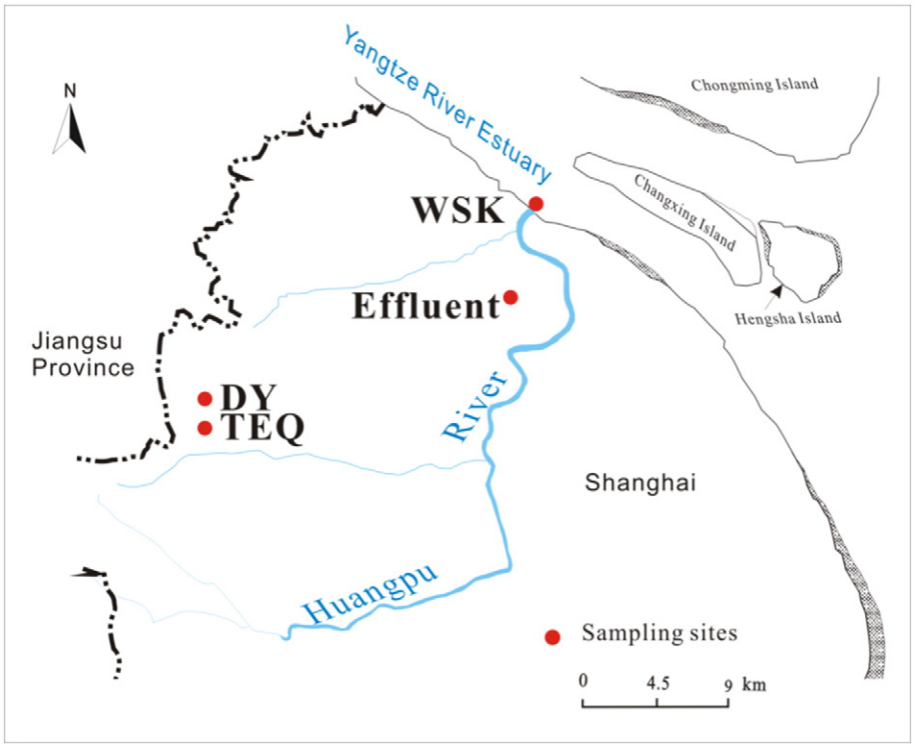

Fig. 1. The sampling sites along Huangpu River in Shanghai, China. (WSK: Wusongkou; Effluent: the effluent of a WWTP in Shanghai; DY: Daying; TEQ: Tianenqiao).

urban WWTP near Huangpu River; Daying (DY) and Tianenqiao (TEQ) are upstream of Huangpu River impacted by livestock, i.e. poultry and swine operations, respectively. Surface water was collected in a 50 L stainless steel bucket which was pre-cleaned sequentially by acetone, deionized water and Milli-Q water. Some general hydrochemical parameters such as pH and dissolved oxygen (DO) were measured during sampling. The water samples were filtered within 24 h through 1 μm glassfiber filters (PAUL, USA), which were held in a 293 mm stainless steel sanitary filter holder (Handwheel Wrench 316 Holder, Millipore).

Colloids were isolated from the bulk water samples (i.e. <1 μm) by a cross-flow ultrafiltration (CFUF, Pellicon System, Millipore, USA) according to the method described in Supplementary Materials, which was equipped with a Millipore 1 kDa regenerated cellulose Pellicon 2 PLAC ultrafiltration membrane (0.5 m^2). Therefore, the colloids in this study were operationally defined as particles between 1 kDa (roughly equivalent to 1 nm in size) and 1 μm, which were used in UV–visible absorption and fluorescence, FlFFF, and AFM analysis. Detailed information on the water sample processing has been provided in the Supplementary materials (Fig. S1). Colloidal concentration (CC) and colloidal organic carbon concentration (COC) were both measured according to the method described in Supplementary Materials.

2.2. UV–visible absorption

Colloids absorbance was measured using a UV–visible spectrophotometer (Shimadzu UV-2600) at a resolution of 0.5 nm between 200 and 800 nm. All samples were ultrasonicated, allowed to reach room temperature and were measured in triplicate in a 1 cm path-length cell with Milli-Q water as the blank. The average sample absorbance within the range 600–800 nm was subtracted from each absorbance scan to correct for offsets due to the instrumental drift and light scattering (Green and Blough, 1994). The measured absorbance at wavelength λ was converted to absorption coefficient α (m^{-1}) according to Eq. (1) (Helms et al., 2008):

$$\alpha_\lambda = \frac{2.303\left(A_\lambda - \overline{A}_{600-800}\right)}{L} \quad (1)$$

where α_λ is the absorption coefficient at wavelength λ (nm) and L (m) is the cell path-length (here 0.01 m). A_λ is the absorbance, while $A_{600-800}$ is the average absorbance between 600 nm and 800 nm. Absorption coefficients at 350 nm (α_{350}), 355 nm (α_{355}) and 412 nm (α_{412}) were chosen to represent the CDOM concentrations, hereinto 355 nm is commonly used as the signal of the chlorophyll fluorescence (Batchelli et al., 2009; Guéguen et al., 2011). $SUVA_{254}$ was calculated by dividing α_{254} (m^{-1}) by the COC concentration (mg L^{-1}), which strongly correlates with the aromaticity of colloids (Weishaar et al., 2003).

2.3. Fluorescence analysis

Fluorescence spectra of colloidal size fractions were recorded with a Hitachi F-4500 fluorescence spectrophotometer using the method described in the Supplementary Materials. The fluorescence intensity was presented in equivalent water Raman units (r.u.). Once the fluorophores of excitation-emission matrix (EEM) were identified, the peak intensity for each fluorophore was located within an area covering the range of known fluorescence for each fluorophore (Section 3.2) (Coble, 1996).

2.4. Flow field-flow fractionation (FlFFF)

A Wyatt Eclipse™ Dualtec asymmetrical FlFFF system (Wyatt Technology, USA) was used to fractionate colloids based on their diffusion coefficient prior detection by fluorescence spectroscopy. Colloids fractionation was performed using a long channel (246 mm) equipped with a 1 kDa polyethersulfone (PES) membrane as an accumulation

Table 1
General hydrochemical parameters and absorbance characteristics of colloids.

	WSK	Effluent	DY	TEQ		WSK	Effluent	DY	TEQ
DO (ppm)	3.6	5	0.6	1.8	S_R	0.98	1.07	1.27	1.17
pH	7.91	6.85	7.66	7.78	E_{250}/E_{365}	5.2	4.11	3.48	3.49
CC (mg L^{-1})	54.8	43.9	90.9	86.8	E_{300}/E_{400}	4.48	3.38	2.75	2.89
COC (mg L^{-1})	0.69	3.93	4.72	8.44	E_{254}/E_{365}	4.94	3.92	3.33	3.38
α_{350} (m^{-1})	11.08	2.63	6.03	6.35	E_{280}/E_{350}	2.91	2.47	2.22	2.26
α_{355} (m^{-1})	10.16	2.55	5.64	5.89	E_{254}/E_{436}	11.92	7.83	6.04	6.85
α_{412} (m^{-1})	4.17	0.94	2.65	3.12	E_{365}/E_{470}	3.42	2.57	2.23	2.63
$SUVA_{254}$ (L mg^{-1} m^{-1})	33.18	2.58	4.35	2.33	E_{465}/E_{665}	3	1.67	1.71	2.5
$S_{275-295}$ (nm^{-1})	0.0143	0.0131	0.0123	0.012	E_{470}/E_{655}	3	1.56	1.63	2.5
$S_{350-400}$ (nm^{-1})	0.0146	0.0123	0.0097	0.0103					

wall. The carrier solution was 1 mM $NaNO_3$ solution. The detailed instrument information of FlFFF and the operational parameters are given in Table S1. In accordance with the colloidal concentration, different sample volumes were injected and focused in the channel for 11 min with a detector flow of 1 mL min^{-1} and a focus flow of 3 mL min^{-1}, followed by elution and fractionation for 29 min with a constant cross-flow of 3 mL min^{-1}. All the water samples were prefiltrated using a 0.45 μm PTFE filters before introduction to the FlFFF channel to remove any large aggregates and avoid steric elution interferences (Baalousha et al., 2006).

Colloids eluting from the FlFFF were analyzed using a fluorescence spectrometer (Agilent 1260 series) with fluorescence at Ex-Em pairs 290/420 nm, 240/360 nm, 290/360 nm and 230/420 nm. The sample recovery was determined comparing the integrated fluorescence signal of colloids under the experimental cross flow to the integrated fluorescence signal of the same colloids without applying any cross flow. A polymer standard 20 ± 2 nm polystyrene particle was introduced to calibrate the channel thickness, enabling calculation of the hydrodynamic diameter distribution of colloids through ISIS software (Wyatt Technology, USA). D_p is defined as the diameter of the peak maximum. The number (D_n) and weight (D_w) average diameters were calculated according to Eqs. (2) and (3) (Yau et al., 1979):

$$D_n = \sum_{i=1}^{n} h_i / \sum_{i=1}^{n} \frac{h_i}{D_i} \quad (2)$$

$$D_w = \sum_{i=1}^{n} h_i D_i / \sum_{i=1}^{n} h_i \quad (3)$$

where h_i is the detector response of the sample at retention time i, and D_i is the diameter at retention time i which is determined from the polymer standard.

2.5. Atomic force microscopy (AFM)

An Asylum Research AFM was used to measure colloid morphologies, size distribution and size polydispersity. All analyses were performed under ambient air conditions. AFM samples preparation is described in Supplementary materials following a method presented

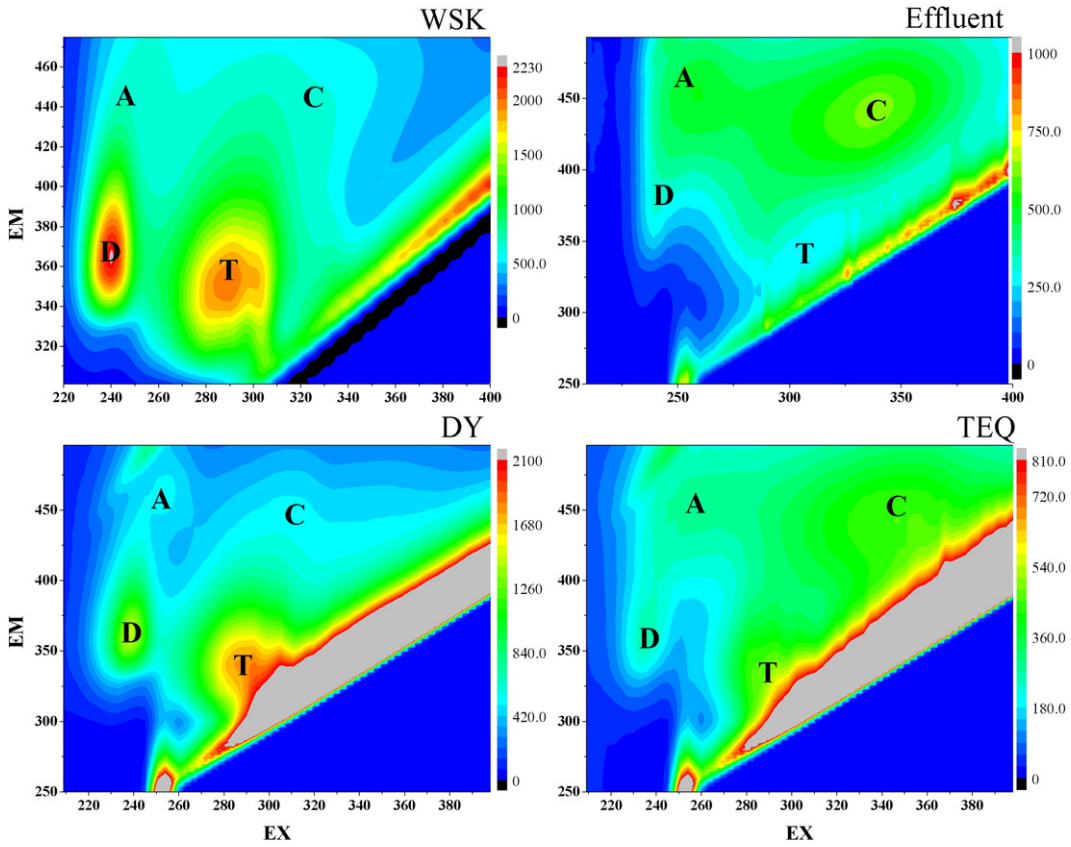

Fig. 2. Fluorescence EEM plot and the fluorescence peak position of the four colloids.

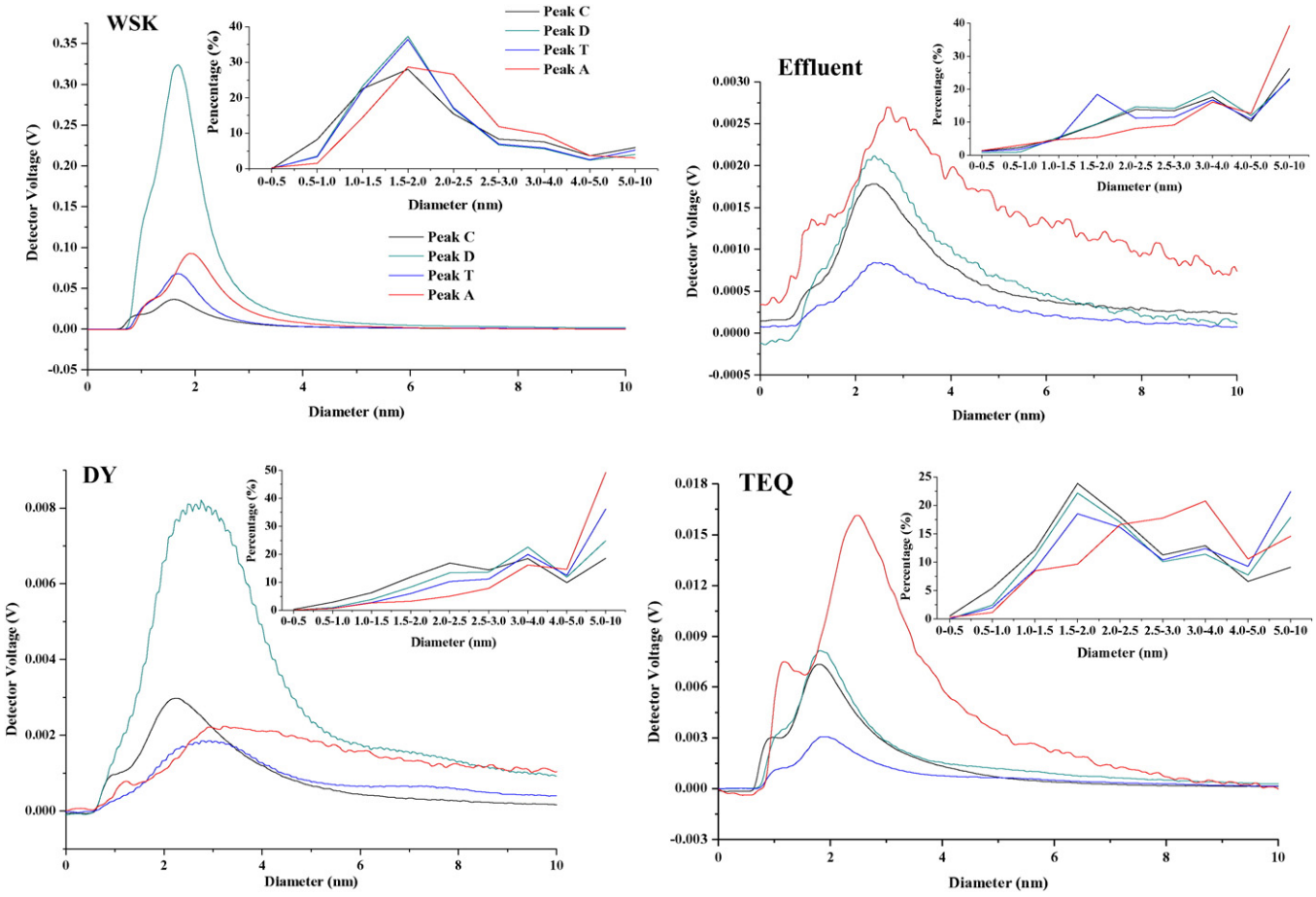

Fig. 3. FlFFF fractograms from the four colloid samples detected at different excitation–emission pairs (Peak C: 290/420 nm; Peak A: 230/420 nm; Peak D: 240/360 nm; Peak T: 290/360 nm). The inset diagrams show the percentage partitioning of the size distribution under different fluorescence wavelengths.

in Baalousha and Lead (2012, 2013). The number N(z) and weight S(z) average sizes were determined according to Eqs. (4) and (5) respectively, and size polydispersity was calculated according to Eq. (6).

$$N(z) = \sum_i n_i z_i / \sum_i n_i \quad (4)$$

$$S(z) = \sum_i n_i z_i^2 / \sum_i n_i z_i \quad (5)$$

$$\text{Polydispersity} = S(z)/N(z) \quad (6)$$

where n_i and z_i is the number and the height of the particle measured, respectively.

2.6. Principal component analysis (PCA)

PCA was employed for data reduction and exploratory analysis. The PCA was carried out in SPSS 19.0 using the parameters obtained in UV–visible absorbance and fluorescence analysis, FlFFF and AFM, including α_{355}, $SUVA_{254}$, the absorbance ratios E_{254}/E_{365}, E_{254}/E_{436}, and E_{465}/E_{665},

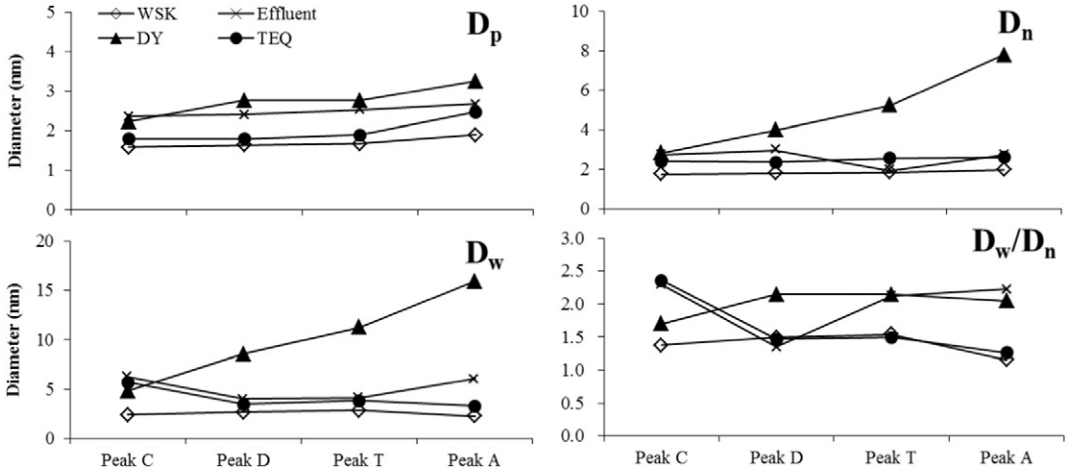

Fig. 4. D_p, D_n, D_w and D_w/D_n of the colloids detected at different fluorescence wavelengths (Peak C: fulvic-like; Peak D: protein-like; Peak T: tryptophan-like; Peak A: humic-like).

maximum intensity of the fluorophores, average value of D_n, D_w, and D_w/D_n at the selected fluorescence wavelengths, N(z), polydispersity, as well as the general hydrochemical parameters (DO, pH, CC, and COC). Each extracted principal components (PCs) represents an independent feature of colloids. KMO and Bartlett's test results are not shown due to the limited number of samples in this study. PCA in this study was only used to extract the latent parameters and to explore the correlations between colloid properties.

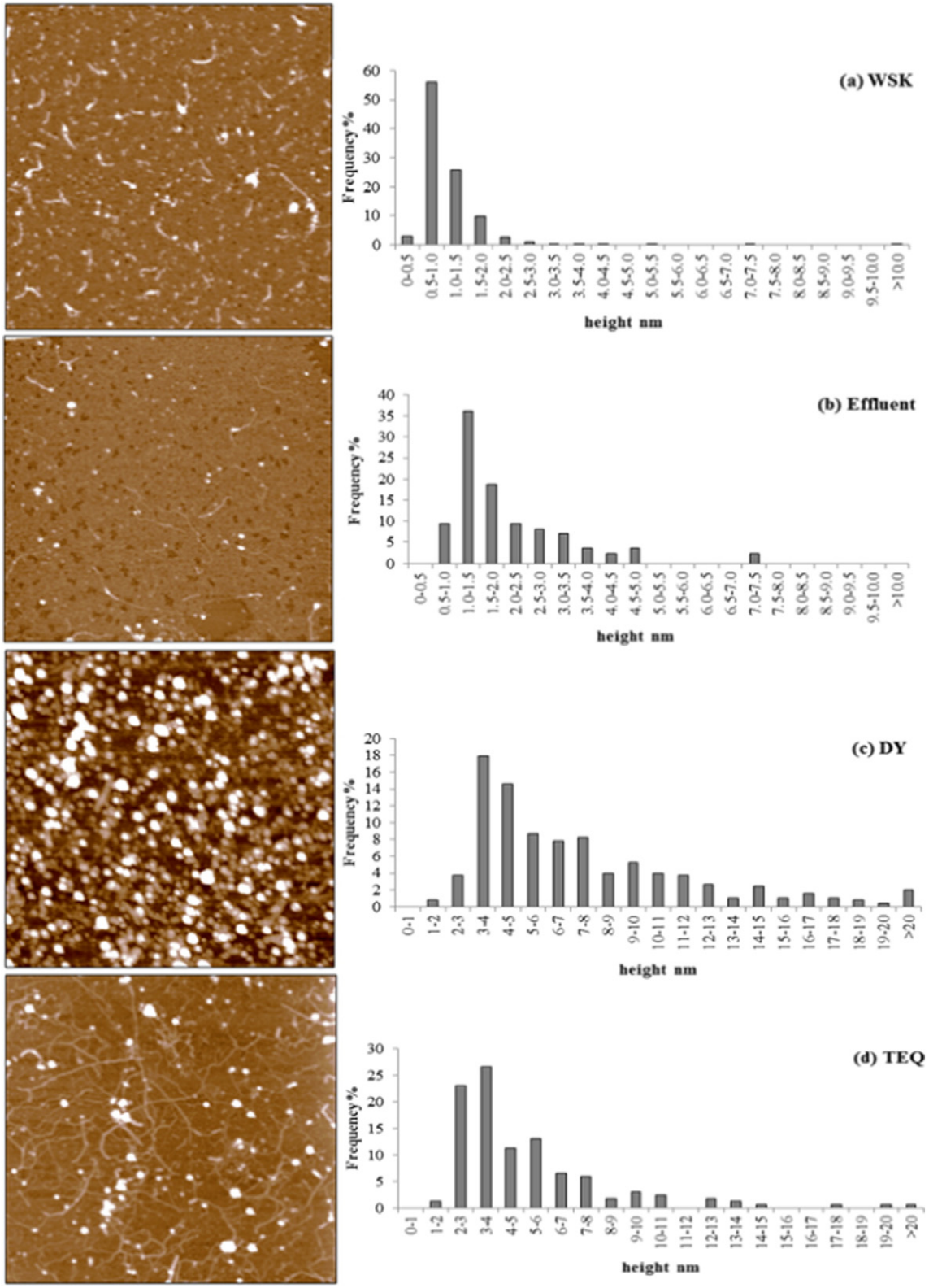

Fig. 5. Typical atomic force microscopy images of colloids and the corresponding number individual particles size distribution.

3. Results and discussion

3.1. General hydrochemical parameters

DO, pH, CC, and COC are shown in Table 1. All the water samples were circumneutral, with pH ranging from 6.85 to 7.91. The DO and CC values were site-specific with the lowest DO and highest CC found in the most contaminated water (DY). A significant negative correlation was found between DO and CC ($R^2 = 0.95$, $P = 0.023$) (Fig. S2a), revealing that the more contaminated water characterized by low DO value has a relatively high CC value. Less significant correlation ($R^2 = 0.42$, $P = 0.356$) was found between CC and COC (Fig. S2a), indicating the different compositions of colloids in the different sources of water.

3.2. UV–vis absorbance

Absorption coefficients at 350 nm (α_{350}), 355 nm (α_{355}) and 412 nm (α_{412}) ranges were 2.63–11.08, 2.55–10.16, and 0.94–4.17 m^{-1} with the highest value found in WSK for all the three wavelengths, indicating the relative high CDOM proportion of colloid in WSK. In addition, α_{350}, α_{355} and α_{412} are strongly correlated with each other ($R^2 > 0.93$) (Fig. S2b and c). Thus, only α_{355} was used in PCA. $SUVA_{254}$ values varied greatly ranging from 2.33 to 33.18 L mg^{-1} m^{-1}, with highest value in WSK. $SUVA_{254} > 4$ L mg^{-1} m^{-1} indicates mainly hydrophobic and aromatic material, while $SUVA_{254} < 3$ L mg^{-1} m^{-1} mainly corresponds to hydrophilic material (Edzwald and Tobiason, 1999; Minor and Stephens, 2008). Therefore, the colloids in WSK are likely to be highly aromatic, whereas those in Effluent, DY and TEQ are likely to be hydrophilic.

Moreover, the absorption spectra increased exponentially with decreasing wavelength and peaked near 213.5 nm for all colloid samples (Fig. S3). To extract more information from these spectra about colloid properties, several absorption ratios were defined in the literature. E_{250}/E_{365}, E_{254}/E_{365} and E_{300}/E_{400} were used as surrogates for colloid size with relatively high values corresponding to smaller colloid sizes (Peuravuori and Pihlaja, 1997; Artinger et al., 2000 Barreto et al., 2003). E_{280}/E_{350} represented the aromatic carbon content of colloids (Croue et al., 2000). In this study, absorption ratios (E_{250}/E_{365}, E_{254}/E_{365} and E_{300}/E_{400} and E_{280}/E_{350}) were highest in WSK, followed by Effluent, TEQ and DY, indicating that smaller particles with higher aromaticity were dominant in the pristine natural water (WSK) compared to those in wastewaters impacted by livestock (DY and TEQ). Because these absorption parameters are thought to be related to colloidal size distribution, it is not surprising that they were positively correlated to each other ($R^2 > 0.99$) (Fig. S2d and e), thus only E_{254}/E_{365} was used in PCA.

E_{254}/E_{436} value was introduced to help estimate the source of colloids (autochthonous vs. terrestrial) (Chin et al., 1994). In this study, E_{254}/E_{436} ratio was 6.0–11.9 within the range of 4–11,suggesting that a greater organic matter content is associated with the presence of humic like substances derived from terrestrial DOM (Battin, 1998). E_{365}/E_{470} represents the presence of UV–visible absorbing functional groups (Stevenson, 1994). A positive correlation was observed between E_{254}/E_{436} and E_{365}/E_{470} ($R^2 = 0.95$, $P = 0.027$) (Fig. S2f), suggesting that the lower E_{365}/E_{470} values referred to the terrestrial colloids. It was in good agreement with the previous study by Ilina et al. (2014), which reported that E_{365}/E_{470} values increased from soil solution towards terminal lake. Finally, the change in degree of humification is reflected in E_{465}/E_{665} and E_{470}/E_{655} (Hur et al., 2006; Ilina et al., 2014). In this study, E_{465}/E_{665} values were much close to E_{470}/E_{655} with values between 1.67 and 3.00, which was within the range of humic acids (the E_{465}/E_{665} ratios for humic acids is usually <5.0) (Chen et al., 1977).

3.3. Fluorescence signatures

The EEM plots of the four colloidal samples are shown in Fig. 2, and four fluorophores proposed by Coble (1996) were identified: fulvic-like fluorescence (peak C, Ex = 300–340 nm, Em = 400–460 nm), protein-like fluorescence (peak D, Ex = 210–230 nm, Em = 340–360 nm), tryptophan-like fluorescence (peak T, Ex = 270–280 nm, Em = 330–370 nm), and humic-like fluorescence (peak A, Ex = 210–250 nm, Em = 400–460 nm). The intensity of the identified fluorophore peaks is shown in Fig. S4. The fluorescence intensity generally decreased as follows: WSK > DY > Effluent > TEQ (Fig. 2). The calculated intensity of fluorophores shows that (Fig. S4), Peak T is the dominant (e.g. highest intensity) for the colloids in DY and TEQ, while peak D and C are the dominant for the colloids in WSK and Effluent.

3.4. Size distribution at different fluorescence in FlFFF

Fig. 3 shows the size distribution of the four colloids measured by FlFFF coupled to a fluorescence detector at selected excitation/emission wavelengths. For WSK and DY, the relatively high signals were found for protein-like fluorescence (peak D); while for Effluent and TEQ, the high signals were found for humic-like fluorescence (peak A). The fluorescence signals were divided into the 0–0.5 nm, 0.5–5 nm and 5–10 nm size ranges. All the fluorescence wavelengths show the majority of fluorescent molecules occurred in the size range of 0.5–5 nm for all colloids. Calculated percentage partitioning of the selected fluorescence (sum of the integrated areas) among the different size fractions (inset image in Fig. 3) suggests that 50–93% colloids occurred in 0.5–5 nm size fraction, while the rest (6.5–50%) occurred almost exclusively in the 5–10 nm size fraction, and negligible amounts (<1.5%) occurred in 0–0.5 nm size fraction. Additionally, each sample was divided into small and large fractions (i.e. small fraction, <2.0 nm; large fraction, >2 nm) (Fig. S5). Results revealed that relative high percentage (18.4–58.9%) of colloids for peak C is in the small size range; in contrast, the higher percentage (55.0–93.1%) is found for peak A in the larger size fraction (Fig. S5). This result is different from that reported by Stolpe et al. (2014), who showed 21–100% percentage of protein-like fluorescent DOM (Ex/Em at 275/305 nm and 275/340 nm) in both small (2–3 nm) and large colloidal fractions (mean hydrodynamic diameter 6–7 nm). These differences in colloid composition could be attributed to the selected fluorescent wavelength. Taken together these results reveal that fluorescence of colloids is size-dependent.

The peak maximum (D_p) from FlFFF analysis was around 1.6–1.9 nm for WSK, 2.4–2.7 nm for Effluent, 2.2–3.3 nm for DY, and 1.8–2.5 nm for TEQ (Table S2). Calculated D_n and D_w values ranged from 1.76 (WSK, peak C) to 7.78 (DY, peak A) and from 2.31 (WSK, peak A) to 15.93 (DY, peak A), respectively (Table S2). Moreover, D_n values were positively correlated to D_p ($R^2 = 0.63$, $P < 0.001$) and D_w ($R^2 = 0.93$, $P < 0.001$) values (Fig. S6), thus only D_p and D_w were used in PCA. Polydispersity (D_w/D_n) in this study varied greatly from 1.16 (WSK, peak A) to 2.36 (TEQ, peak C) (Fig. 4). D_p, D_n and D_w values generally increased in the order of peak C < peak D < peak T < peak A, which was more obvious in DY and there was no clear trend of size polydispersity among the different samples (Figs. 4 and S7, and Table S2). Obviously, this trend that the relative small and large colloidal size was obtained at peak C and peak A, respectively, was congruent with the result of percentage partitioning of fluorescence in the size fractions (Fig. 3, the inset image and Fig. S5), which further confirmed that fluorescence of colloids is size-dependent.

Table 2
Summary of samples' physicochemical parameters under AFM.

Samples	N(z)	S(z)	Poplydispersity
WSK	1.09	1.73	1.59
Effluent	2.07	2.94	1.42
DY	7.17	10.37	1.45
TEQ	5.01	7.01	1.40

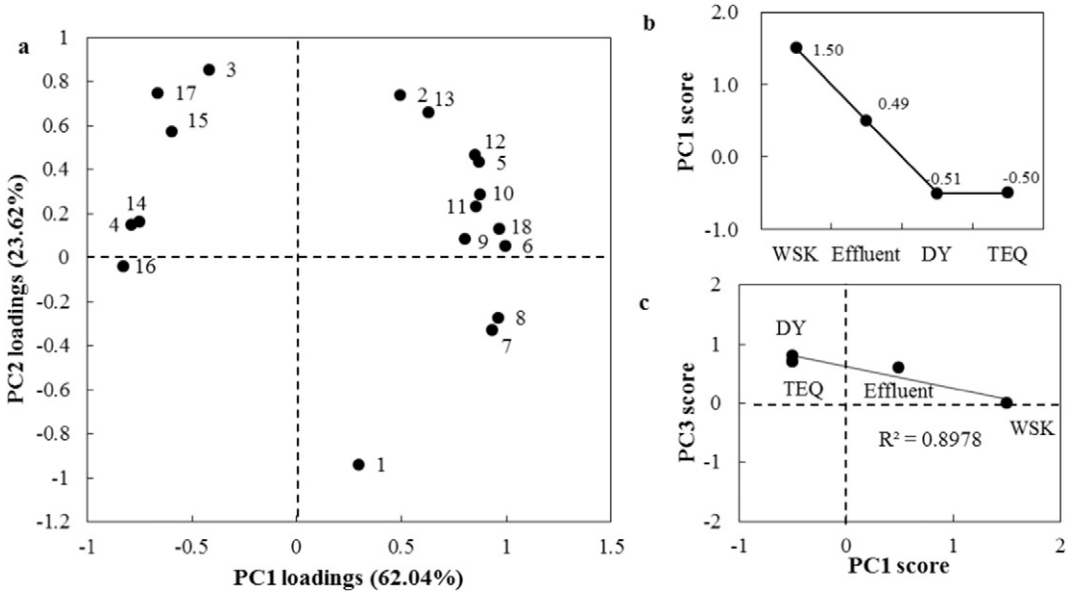

Fig. 6. Results of principal component analysis (PCA). (a) Loadings plots for PC1 and PC2. Numbers are for: (1) DO, (2) pH, (3) CC, (4) COC, (5) α_{355}, (6) $SUVA_{254}$, (7) E_{254}/E_{365}, (8) E_{254}/E_{436}, (9) E_{465}/E_{665}, (10 − 13) peak C, A, D, and T, (14) D_p, (15) D_w, (16) D_w/D_n, (17) N(z), and (18) polydispersity. (b) Sample scores for PC1. (c) Scores plotting for PC1 and PC3.

3.5. Morphology and colloidal size distribution by AFM

Representative AFM images and the corresponding particle size distribution (i.e. the height above the substrate surface) of the four colloidal samples are shown in Fig. 5. Images from WSK, Effluent and TEQ show networks of fibrils and intimate associations with the roughly spherical material. Moreover, these fibrils were 300–500 nm in length in WSK, whereas >2 μm in TEQ; and the height of these fibrils ranged from 0.2 nm to 2 nm. In natural waters, fibrillar polymers such as aquagenic polysaccharides and peptidoglycans are likely to be the major components of COC. Such COC is most likely formed due to the production of exudates or the decomposition of structural polysaccharides (Wilkinson et al., 1999). Colloids in DY were predominantly individual, spherical particles with no fibrils.

AFM size distribution histograms show the large majority of the observed particles is <2 nm for WSK (95%), 5 nm for Effluent (98%), 13 nm for DY (81%) and 10 nm for TEQ (92%). Number-average height (N(z)) increased in the following order: WSK (1.09) < Effluent (2.07) < TEQ (5.01) < DY (7.17) (Table 2). Obviously, colloid sizes measured by AFM and FlFFF followed the same trend i.e. WSK < Effluent < TEQ < DY. Nonetheless, WSK and Effluent colloid size measured by AFM were smaller than those measured by FlFFF, whereas DY and TEQ colloid size measured by FlFFF and AFM were similar. This differences in colloid sizes measured by FlFFF and AFM among different sites could be attributed to the particle structure, i.e. colloids from DY and TEQ are likely to be hard spheres as the sizes measured by AFM and FlFFF are similar, thus validating Stokes Einstein assumption, whereas colloids from WSK and Effluent are either nonspherical or permeable as the sizes measured by AFM are smaller than those measured by FlFFF, indicating a deviation from Stokes Einstein assumption (Baalousha and Lead, 2007a, Baalousha and Lead, 2012).

3.6. Principal component analysis (PCA)

The first three principal components (PC1-3) were sufficient to explain the properties of colloids, accounting for 60.77%, 23.76%, and 15.48% of the total variance, respectively. All parameters derived from absorbance and fluorescence analysis (including α_{355}, $SUVA_{254}$, the absorbance ratios E_{254}/E_{365}, E_{254}/E_{436}, and E_{465}/E_{665}, and the maximum fluorescence intensity of peak C, D, T, and A) had positive weightings on PC1 (Fig. 6a). These loadings reflected the optical properties of parameters in the colloids. In PC2, pH and CC had the maximum positive loadings, while that of DO was negative, indicating the important role played by the environmental factors. In PC3, the top positive loading was for D_p, D_w, and D_w/D_n, which were the parameters of size distribution obtained from FlFFF. Plotting the colloid samples scores for PC1 revealed that samples ordered by optical properties, with more absorbance and fluorescent materials in WSK (Fig. 6b). Furthermore, although limited data, a declining trend was observed in the plotting of scores matrix for PC1 and PC3 ($R^2 = 0.90$) (Fig. 6c), indicating that the relatively small colloids have more absorbance and fluorescence materials.

4. Conclusions

Characterization of colloids from pristine and human impacted surface waters was conducted by applying multiple-method perspectives and tools. Colloids exhibited considerable variability in absorbance and fluorescence characteristics and size distribution. Moreover, colloids in pristine natural river water showed higher aromaticity and humification, higher fluorescent intensity, and smaller size than those in wastewaters impacted by livestock. Colloid size detected at different fluorescence wavelengths by FlFFF showed that the fluorescence characteristic was size-dependent. Similar results were found in PCA, which indicates that latent parameters related to optical properties depend on the latent parameters reflecting size distribution.

The analytical techniques used in this study have potential for wider applications in studying the occurrence and fate of natural and engineered nanoscale particles in the aquatic environments. Additionally, because the behavior of pollutants depends not just on a single colloid property, but rather on the combination of properties of colloids, the complementary methods in this work also have potential applications for understanding the impact of colloids on the fate and transport of pollutants. However, the possibility of such consistent relationships should be investigated much further to allow accurate statistical predictions to be made.

Acknowledgments

This study was funded by the National Natural Science Foundation of China (41371451; 41271473; 41130525). Additional support was

provided by the Open Foundation of East China Normal University, Open Foundation of State Key Laboratory of Poyang Lake Wetland and Watershed Research, Ministry of Education, Jiangxi Normal University (PK2015006), and Science and Technology Research Project of Education Department of Jiangxi Province (GJJ150307). We also acknowledge the financial support from the Smartstate Center for Environmental Nanoscience and Risk at University of South Carolina.

Appendix A. Supplementary data

Supplementary data to this article can be found online at http://dx.doi.org/10.1016/j.scitotenv.2016.02.198.

References

Artinger, R., Buckau, G., Geyer, S., Fritz, P., Wolf, M., Kim, J.I., 2000. Characterization of groundwater humic substances: influence of sedimentary organic carbon. Appl. Geochem. 15, 97–116.
Baalousha, M., Lead, J.R., 2007a. Characterization of natural aquatic colloids (<5 nm) by flow-field flow fractionation and atomic force microscopy. Environ. Sci. Technol. 41, 1111–1117.
Baalousha, M., Lead, J.R., 2007b. Size fractionation and characterization of natural aquatic colloids and nanoparticles. Sci. Total Environ. 386, 93–102.
Baalousha, M., Lead, J.R., 2012. Rationalizing nanomaterial sizes measured by atomic force microscopy, flow field-flow fractionation, and dynamic light scattering: sample preparation, polydispersity, and particle structure. Environ. Sci. Technol. 46, 6134–6142.
Baalousha, M., Lead, J.R., 2013. Characterization of natural and manufactured nanoparticles by atomic force microscopy: effect of analysis mode, environment and sample preparation. Colloid Surf. A: Physicochem. Eng. Asp. 419, 238–247.
Baalousha, M., Kammer, F.V.D., Motelica-Heino, M., Hilal, H.S., Coustumer, P.L., 2006. Size fractionation and characterization of natural colloids by flow-field flow fractionation coupled to multi-angle laser light scattering. J. Chromatogr. A 1104, 272–281.
Barreto, S.R.G., Nozaki, J., Barreto, J.W., 2003. Origin of dissolved organic carbon studied by UV–vis spectroscopy. Acta Hydrochim. Hydrobiol. 31, 513–518.
Batchelli, S., Muller, F.L.L., Baalousha, M., Lead, J.R., 2009. Size fractionation and optical properties of colloids in an organic rich estuary (Thurso, UK). Mar. Chem. 113, 227–237.
Battin, T.J., 1998. Dissolved organic matter and its optical properties in a black water tributary of the upper Orinoco river, Venezuela. Org. Geochem. 28, 561–569.
Boehme, J., Wells, M., 2006. Fluorescence variability of marine and terrestrial colloids: examining size fractions of chromophoric dissolved organic matter in the Damariscotta River estuary. Mar. Chem. 101, 95–103.
Bouby, M., Geckeis, H., Geyer, F.W., 2008. Application of asymmetric flow field-flow fractionation (AsFlFFF) coupled to inductively coupled plasma mass spectrometry (ICPMS) to the quantitative characterization of natural colloids and synthetic nanoparticles. Anal. Bioanal. Chem. 392, 1447–1457.
Buzea, C., Pacheco, I.I., Robbie, K., 2007. Nanomaterials and nanoparticles: sources and toxicity. Biointerphases 2, MR17–MR71.
Chen, Y., Senesi, N., Schnitzer, M., 1977. Information provided on humic substances by E4/E6 ratios. Soil Sci. Soc. Am. J. 41, 352–358.
Chin, Y.P., Aiken, G., O'Loughlin, E., 1994. Molecular weight, polydispersity, and spectroscopic properties of aquatic humic substances. Environ. Sci. Technol. 28, 1853–1858.
Coble, P.G., 1996. Characterization of marine and terrestrial DOM in seawater using excitation-emission matrix spectroscopy. Mar. Chem. 51, 325–346.
Croue, J.P., Violleau, D., Labouyrie, L., Krasner, S.W., Amy, G.L., 2000. Disinfection byproduct potentials of hydrophobic and hydrophilic natural organic matter fractions: a comparison between and low-and high-humic water. In: Barrett, S. (Ed.), Natural Organic Matter and Disinfection By-Products. American Chemical Society Symposium 761, Washington, D.C., pp. 139–153.
Cuss, C.W., Guéguen, C., 2015. Relationships between molecular weight and fluorescence properties for size-fractionated dissolved organic matter from fresh and aged sources. Water Res. 68, 487–497.
Edzwald, J.K., Tobiason, J.E., 1999. Enhanced coagulation: US requirements and a broader view. Water Sci. Technol. 40, 63–70.
Green, S.A., Blough, N.V., 1994. Optical absorption and fluorescence properties of chromophoric dissolved organic matter in natural waters. Limnol. Oceanogr. 39, 1903–1916.
Guéguen, C., Cuss, C.W., 2011. Characterization of aquatic dissolved organic matter by asymmetrical flow field-flow fractionation coupled to UV–visible diode array and excitation emission matrix fluorescence. J. Chromatogr. A 1218, 4188–4198.
Guéguen, C., Granskog, M.A., McCullough, G., Barber, D.G., 2011. Characterization of colored dissolved organic matter in Hudson Bay and Hudson Strait using parallel factor analysis. J. Mar. Sys. 88, 423–433.
Hassellöv, M., 2005. Relative molar mass distributions of chromophoric colloidal organic matter in coastal seawater determined by Flow Field-Flow Fractionation with UV absorbance and fluorescence detection. Mar. Chem. 94, 111–123.
Helms, J.R., Stubbins, A., Ritchie, J.D., Minor, E.C., 2008. Absorption spectral slopes and slope ratios as indicators of molecular weight, source, and photobleaching of chromophoric dissolved organic matter. Limnol. Oceanogr. 53, 955–969.
Hong, H.S., Yang, L.Y., Guo, W.D., Wang, F.L., Yu, X.X., 2012. Characterization of dissolved organic matter under contrasting hydrologic regimes in a subtropical watershed using PARAFAC model. Biogeochemistry 109, 163–174.
Huguet, A., Vacher, L., Saubusse, S., Etcheber, H., Abril, G., Relexans, S., Ibalot, F., Parlanti, E., 2010. New insights into the size distribution of fluorescent dissolved organic matter in estuarine waters. Org. Geochem. 41, 595–610.
Hur, J., Williams, M.A., Schlautman, M.A., 2006. Evaluating spectroscopic and chromatographic techniques to resolve dissolved organic matter via end member mixing analysis. Chemosphere 63, 387–402.
Ilina, S.M., Drozdova, O.Y., Lapitskiy, S.A., Alekhin, Y.V., Demin, V.V., Zavgorodnyaya, Y.A., Shirokova, L.S., Viers, J., Pokrovsky, O.S., 2014. Size fractionation and optical properties of dissolved organic matter in the continuum soil solution-bog-river and terminal lake of a boreal watershed. Org. Geochem. 66, 14–24.
Kalmykova, Y., Björklund, K., Strömvall, A.M., Blom, L., 2013. Partitioning of polycyclic aromatic hydrocarbons, alkylphenols, bisphenol A and phthalates in landfill leachates and stormwater. Water Res. 47, 1317–1328.
Khalaf, M., Kohl, S.D., Klumpp, E., Rice, J.A., Tombacz, E., 2003. Comparison of sorption domains in molecular weight fractions of a soil humic acid using solid-state 19FNMR. Environ. Sci. Technol. 37, 2855–2860.
Laborda, F, Ruiz-Begueria, S., Bolea, E., Castillo, J.R., 2011. Study of the size-based environmental availability of metals associated to natural organic matter by stable isotope exchange and quadrupole inductively coupled plasma mass spectrometry coupled to asymmetrical flow field flow fractionation. J. Chromatogr. A 1218, 4199–4205.
Lapworth, D.J., Stolpe, B., Williams, P.J., Gooddy, D.C., Lead, J.R., 2013. Characterization of suboxic groundwater colloids using a multi-method approach. Environ. Sci. Technol. 47, 2554–2561.
Lead, J.R., Wilkinson, K.J., 2006. Aquatic colloids and nanoparticles: current knowledge and future trends. Environ. Chem. 3, 159–171.
Liu, R., Lead, J.R., Baker, A., 2007. Fluorescence characterization of cross flow ultrafiltration derived freshwater colloidal and dissolved organic matter. Chemosphere 68, 1304–1311.
Minor, E., Stephens, B., 2008. Dissolved organic matter characteristics within the Lake Superior watershed. Org. Geochem. 39, 1489–1501.
Moon, J., Kim, S.H., Cho, J., 2006. Characterizations of natural organic matter as nanoparticle using flow field-flow fractionation. Colloids Surf. A: Physicochem. Eng. Asp. 287, 232–236.
Ngueleu, S.K., Grathwohl, P., Cirpka, O.A., 2013. Effect of natural particles on the transport of lindane in saturated porous media: laboratory experiments and model-based analysis. J. Contam. Hydrol. 149, 13–26.
Nie, M.H., Yang, Y., Zhang, Z.J., Yan, C.X., Wang, X.N., Li, H.J., Dong, W.B., 2014a. Degradation of chloramphenicol by thermally activated persulfate in aqueous solution. Chem. Eng. J. 246, 273–382.
Nie, M.H., Yang, Y., Liu, M., Yan, C.X., Shi, H., Dong, W.B., Zhou, J.L., 2014b. Environmental estrogens in a drinking water reservoir area in Shanghai: occurrence, colloidal contribution and risk assessment. Sci. Total Environ. 487, 785–791.
Persson, T., Wedborg, M., 2001. Multivariate evaluation of the fluorescence of aquatic organic matter. Analytica. Chimica. Acta. 434, 179–192.
Peuravuori, J., Pihlaja, K., 1997. Molecular size distribution and spectroscopic properties of aquatic humic substances. Analytica. Chimica. Acta. 337, 133–149.
Stevenson, F.J., 1994. Humus Chemistry: Genesis, Composition, Reactions. second ed. Wiley, New York, p. 496.
Stolpe, B., Hassellöv, M., Andersson, K., Turner, D.R., 2005. High resolution ICPMS as an online detector for flow field-flow fractionation; multi-element determination of colloidal size distributions in a natural water sample. Anal. Chim. Acta 535, 109–121.
Stolpe, B., Zhou, Z., Guo, L., Shiller, A.M., 2014. Colloidal size distribution of humic-and protein-like fluorescent organic matter in the northern Gulf of Mexico. Mar. Chem. 164, 25–37.
Thurman, E.M., 1985. Organic Geochemistry of Natural Waters. Nijhoff, M., Junk, W., Publishers.
Weishaar, J., Aiken, G.R., Bergamaschi, B.A., Fram, M.S., Fujii, R., Mopper, K., 2003. Evaluation of specific ultraviolet absorbance as an indicator of the chemical composition and reactivity of dissolved organic carbon. Environ. Sci. Technol. 37, 4702–4708.
Wilkinson, K.J., Lead, J.R., 2007. Environmental Colloids and Particles IUPAC.
Wilkinson, K.J., Balnois, E., Leppard, G.G., Buffle, J., 1999. Characteristic features of the major components of freshwater colloidal organic matter revealed by transmission electron and atomic force microscopy. Colloids Surf. A: Physicochem. Eng. Asp. 155, 287–310.
Wyatt, T., Jenkinson, I., Malej, A., 1998. How viscoelastic properties of colloids, transparent exopolymeric particles and marine organic aggregates, modify turbulence and plankton biodynamics in the sea. Progress and Trends in Rheology V 65–66.
Yan, C.X., Yang, Y., Nie, M.H., Gu, L.J., Liu, M., Zhou, J.L., 2015. Selected emerging organic contaminants in Yangtze Estuary water: the importance of colloids. J. Hazard. Mater. 283, 14–23.
Yang, Y., Colman, B.P., Bernhardt, E.S., Hochella, M.F., 2015. Importance of a nanoscience approach in the understanding of major aqueous contamination scenarios: case study from a recent coal ash spill. Environ. Sci. Technol. 49, 3375–3382.
Yau, W.W., Kirkland, J.J., Bly, D.D., 1979. Modern size-exclusion liquid chromatography: practice of gel permeation and gel filtration chromatography. Wiley.
Zanardi-Lamardo, E., Moore, C.A., Zika, R.G., 2004. Seasonal variation in molecular mass and optical properties of chromophoric dissolved organic material in coastal waters of southwest Florida. Mar. Chem. 89, 37–54.